Electronic Supplementary Information (ESI)

Low energy intensity production of fuel-grade bio-butanol enabled by membrane-based extraction †

Ji Hoon Kim [a], Marcus Cook [a], Ludmila Peeva [a], Jet Yeo [a], Leslie W. Bolton [b], Young Moo Lee [c], and Andrew G. Livingston*[a,d]

[a] Barrer Centre, Department of Chemical Engineering, Imperial College London, London, SW7 2AZ, U.K.

[b] BP plc, Chertsey Road, Sunbury-on-Thames, Middlesex TW16 7LN, U.K.

[c] Department of Energy Engineering, Hanyang University, Seoul, 04763, Republic of Korea

[d] School of Engineering and Materials Science, Queen Mary University of London, London, E1 4NS, U.K

Table S1 Properties of gasoline, diesel and bio-alcohols.[1-3]

Property	gasoline	diesel	ethanol	n-butanol	n-pentanol
Energy density (MJ L^{-1})	32	43	26	33	34
Kinematic viscosity (cSt at 40 °C)	0.2 – 0.3	2.42 – 4.0	1.08 – 1.5	2.22 – 2.63	2.89
Latent Heat of Vaporization (kJ kg^{-1})	380 – 500	260 – 270	840 – 918	581 – 586	308
Self ignition temperature (°C)	246 – 280	254 – 300	420	345	300
Flash point (°C)	13	55 – 88	13 – 17	30 – 37	49
Cold flow plugging point (°C)	- 10	- 17 – - 5	< - 51	< - 51	- 40
Lubricity (μm)		315	1057	591	670
Cetane number	5 – 20	40 – 55	8 – 11	17 – 25	18 – 20
Vapor Pressure (kPa at 20 °C)	7.0 – 7.8	0.2 – 0.7	5.95	0.5	0.6
Research octane number	92 – 98	- 25	107	96	78

S1. Comparison of product recovery systems

Conventional dehydration processes such as gas stripping and pervaporation have relatively higher alcohol productivity than extractive recovery systems such as liquid-liquid extraction and perstraction, however, they have limited selectivity. The selectivity ($^{\alpha_{ab}}$), which is a fractional ratio of the desirable product in feed and permeate solutions (upstream and downstream),can be represented by **eqn (S1)**:

$$\alpha_{ab} = \frac{y_a / (1 - y_a)}{x_a / (1 - x_a)} \tag{S1}$$

where x_a and y_a are the fraction of the desirable product in feed and permeate solutions. Based on selectivity, a purity of the final product in permeate solution can be calculated as followed **eqn (S2)**:

$$y_a = \frac{\left(\frac{x_a}{1 - x_a}\right) \cdot \alpha_{ab}}{1 + \left(\frac{x_a}{1 - x_a}\right) \cdot \alpha_{ab}} \tag{S2}$$

Table S2 Butanol recovery performance of membrane-based processes: pervaporation and perstraction with different membrane types: thin-film composite (TFC), hollow fiber, and tubular membranes, and operating temperatures.[4-15]

Application	Material	Type	Feed (*wt*%)	Separation factor	Purity	Temp. (°C)	n-BuOH flux (g m^{-2} h^{-1})	Reference
Pervaporation	PDMS / ZIF-8	TFC	1	56.9	0.36	80	400.4	J. Mater. Chem. A, 2014, 2, 20947
	PDMS	TFC	1.5	43.7	0.40	55	267.9	Green Chem., 2013, 15, 2180
	Silicate / silicone	TFC	1	85.9	0.46	30	29.2	J. Membr. Sci., 2001, 192, 231
	PTMS	TFC	1	52	0.34	25	20.7	J. Membr. Sci., 2001, 186, 205
	CMX-GF-010-D	TFC	1	39	0.28	37	93.3	Desalination, 2009, 241, 201
	PDMS / PE	TFC	1	34	0.26	37	24.3	J. Membr. Sci., 2010, 363, 287
	PEBA / ZIF-71	TFC	1	18.8	0.16	37	96.8	J. Membr. Sci., 2013, 446, 181
	PERVAP-2200	TFC	1	10	0.09	37	30.3	J. Membr. Sci., 2006, 280, 278
	PEBA / ceramic HF	Hollow fiber	1	20	0.17	30	168.1	J. Membr. Sci., 2016, 510, 338
	PDMS / ceramic HF	Hollow fiber	1	42.9	0.30	30	387.6	J. Membr. Sci., 2014, 450, 38
Perstraction	PDMS / Oleyl alcohol	Tubular	1	> 4000	0.99	37	1	Bioprod. Process, 2005, 83, 43
	PDMS / $[P_{6,6,6,14}][DCA]$	Tubular	1	64.3	0.39	37	4.3	J. Membr. Sci., 2017, 537, 337
	XSPAES / 2-ethyl-1-hexanol	TFC	1	> 4000	0.99	37	55	This work

A selectivity higher than unity means that the desirable product is concentrated in the permeate. For biofuel, the final purity should be higher than 99.5%. Considering that higher alcohols (C > 3) have heterogeneous azeotrope relationships with water, energy-efficient recovery and distillation systems are required. Therefore, to provide a fair comparison of the recovery systems, purity of the final products is calculated in **Table S2**. Although selectivity of the conventional processes slightly decreases according to duration time due to decreasing feed concentration, the purity of the recovered

alcohol against water was simply calculated with a constant feed concentration (10 L of 1 *wt*% n-butanol aqueous solution) and selectivity.

The energy consumption for each of the processes was compared only for recovering the produced alcohols from the fermentation broth, excluding the energy requirements for fermentation and heating to maintain the system temperature at 37 °C, which all processes share in common, and which is negligible compared to the energy requirements of recovery processes. For example, based on the heat capacity of water, the energy required for heating the feed solution (10 L) from 22 ^{o}C to 37 ^{o}C is estimated to be around 0.6 MJ assuming the fermentation starts at room temperature (22 ^{o}C). For the dehydration processes, the required energy for recovery was estimated by energy consumptions of pump and condenser.[16, 17] After enrichment, the energy requirements for heterogeneous azeotrope vacuum distillation was obtained from A.P. Mariano's work (designed by Aspen Plus v7.1 with two units of 10 stage columns and a decanter) depending on the feed composition of each process (**Table S3**).[18] In contrast, for the extractive recovery processes such as liquid-liquid extraction (LL) and perstraction (PS), the required energies for the recovery systems were almost negligible because the processes do not require the energy-intensive condenser and vacuum pump. For the generation of fuel grade alcohol from the extractants, the thermodynamics of the processes were simulated using the NRTL (Non-Random Two Liquid) model in Aspen Plus v8.4. The component properties of n-butanol and 2-ethyl-1-hexanol were defined using the Aspen database. Oleyl alcohol was simulated as the hypothetical component with component properties such as critical temperature, critical pressure, critical volume, and acentricity predicted using UNIFAC. A distillation column was simulated as representational of a distillation process to produce fuel-grade butanol (>99.5 *wt*%). The process flow diagram is illustrated in **Fig. S1**. The distillation column was modelled using Aspen RadFrac distillation with specifications such as (a) a single unit of a 10 stage column, (b) a fresh feed entering above the 5th stage, (c) 40 mmHg of the column pressure, and (d) distillate going through the total condenser. N-butanol (>99.5 *wt*%) is obtained from the distillate through the condenser and extractant

(oleyl alcohol for LL or 2-ethyl-1-hexanol for PS) is obtained from the bottom. The distillate to feed ratio and reflux ratio are adjusted to achieve target butanol purity. The distillate to feed ratio is determined by the molar concentration of butanol at the feed stream, while reflux ratio was changed iteratively to achieve the lowest value required to produce butanol (>99.5 wt%) as high reflux ratio would result in excessive energy usage. The fuel-grade n-butanol is obtained from the column top (52.7 °C at 40mmHg). The specific energy requirement for butanol production (MJ kg^{-1}) was calculated by dividing the total duty of reboiler and condenser by the mass flow rate of butanol at the distillate.

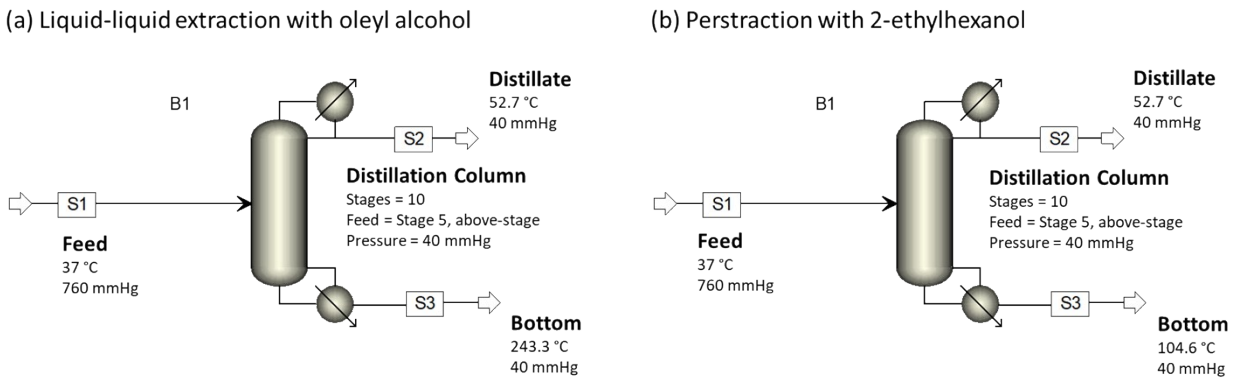

Fig. S1 Process diagram for distillation of fuel-grade butanol from extractive recovery systems such as liquid-liquid extraction and perstraction.

Table S3 A comparison of energy consumptions (MJ kg^{-1}) for n-butanol batch production by recovery systems including gas stripping, pervaporation, liquid-liquid extraction, and perstraction.[16-21]

Property	Dehydration process		Extractive recovery	
	Gas stripping	Pervaporation	Liquid-liquid extraction	Perstraction
Feed	10 L 1*wt*% n-butanol aqueous solution		10 L 1*wt*% n-butanol aqueous solution	
Productivity (g L^{-1} h^{-1})	< 1.0 [a]	5.0 [g]	< 1.0 [b]	5.5 [g]
Selectivity (n-butanol/water)	< 50	< 250 [f]	> 4000	> 4000
Purity of the recovered alcohol in water (%)	12	30	99.9	99.9
Pump (MJ kg^{-1})	0.09 [d]	0.018 [d]	-	0.0007 [e]
Condensation (MJ kg^{-1})	4.67 [d]	4.67 [d]	-	-
Distillation (MJ kg^{-1})	24.7 [f]	12.3 [f]	25.7 [h]	3.9 [h]
Total energy consumption (MJ kg^{-1})	29.4	17.0	25.7	3.9
Literature data (MJ kg^{-1}) [a]	< 30	< 140	< 10	< 10
Literature data (MJ kg^{-1}) [b]	< 31	< 145	< 9	< 9
Literature data (MJ kg^{-1}) [c]	< 150	< 40	< 25	< 25

[a] P. Jimenez-Bonilla, Y. Wang, *Crit. Rev. Biotechnol.*, 2018, **38**, 469-482

[b] C. Xue *et al.*, *Biotechnol. Adv.*, 2013, **31**, 1575-1584

[c] V. Outram *et al.*, *Bioresource Technol.*, 2016, **220**, 590-600, the energy consumption was calculated for ABE production.

[d] M. Matsumura *et al.*, *Bioprocess Eng.,* 1988, **3**, 93-100

[e] J.A. Gil *et al*., *Desalination*, 2010, **250**, 997-1001

[f] A.P. Mariano *et al*., *Energy & Fuels*, 2011, **25**, 2347-2355

[g] Productivity (g L^{-1} h^{-1}) of pervaporation and perstraction is calculated based on the average flux of pervaporation TFC membranes at 37 ^{o}C (**Table S2**) and the developed xSPAES membrane in this work under the same assumptions with 10 L fermentation broth and 1 m^2 membrane area.

[h] Aspen simulation results using NRTL (Non-Random Two Liquid) model with 5 L oleyl alcohol and 0.1 L 2-ethyl-1-hexanol for LL and PS in a batch system, respectively (**Section S1**).

Table S4 The specific energy requirements for the extractive recovery processes such as liquid-liquid extraction and perstraction depending on different volume ratio of extractant and feed solutions with 99% recovery rate of the saturation concentration as a batch system. The detailed information for simulation is described in **Section S5** and **Table S7**.

	Parameters	Liquid-liquid extraction		Perstraction			
Feed stream	V_{Ex}/V_{Fe}	0.5	1.0	0.001	0.01	0.3	1.0
	V_{Ex} (L)	5	10	0.01	0.1	3	10
	Feed concentration (g L^{-1})	15.0	7.8	91.22	84.24	24.29	8.94
	Feed stream rate (g h^{-1})	10		0.0184	0.0199	0.0689	0.1873
Distillation Column	Distillate to feed (mol%)	0.0537	0.0284	0.1791	0.1664	0.0505	0.0188
	Reflux ratio	0.15	0.2	0.4	0.4	1.0	5.0
	Distillate rate (g h^{-1})	151.12	79.42	1.66	1.66	1.7	1.7
	Distillation column temperature (°C)	52.67		52.67			
	Reboiler temperature(°C)	246.82		104.5			
	n-butanol purity from distillate (wt%)	99.9	99.9	99.6	99.7	99.7	99.7
Duty	Reboiler (kJ h^{-1})	3768.95	3805.9	4.51	4.77	14.05	39.35
	Condenser (kJ h^{-1})	-118.69	-65.10	-1.59	-1.58	-2.27	-6.81
Total	Specific butanol production energy (MJ kg^{-1})	25.73	48.74	3.69	3.85	9.87	27.84

S2. Investigation of desirable extractants.

Partition coefficients of extractants were measured by the shake-flask method described in OECD guideline 107 at 37 °C. 100 ml of 5,000 ppm alcohol solutions in water and each extractant were prepared at 37 °C. Water and extractant were vigorously mixed in a vial and left to stand for one day at 37 °C until the phase separation occurred between water and extractant. The concentration in each solvent was measured by gas chromatography with a flame ionization detector (GC-FID 6850, Agilent, USA) and HP-5 column (19095J-323E, Agilent). The column was heated at 15 °C min^{-1} from 40 to 180 °C. The aqueous solution was measured after solvent extraction with dichloromethane. 1 ml aqueous solution was mixed with 1 ml dichloromethane in a 2 ml vial and the dichloromethane fraction was tested. Standard curves for all the alcohols in extractants and water were prepared at 1000, 2500,

5000, and 10,000 ppm concentration. All the standard curves were prepared with higher R^2 value than 0.995 in **Appendix S2 – S4**.

Table S5 Properties of extractants.[22, 23]

Extractant	CAS No.	Partition coefficient at 37 °C to n-BuOH [a]	Molecular weight (g mol^{-1})	Density at 20 °C (g cm^{-3})	Viscosity at 20 °C (cP)	Boiling point at 1 bar (°C)	Melting point at 1 bar (°C)	Heat Capacity at 25 °C (J g^{-1} K^{-1})	Cost (£ kg^{-1})
Oleyl alcohol	143-28-2	3.6 ± 0.18	268.5	0.85	28.3	305 - 370	13 – 19	8.96 [b]	1300 [d] / 50.8
2-ethyl-1-hexanol	104-76-7	9.3 ±0.54	130.2	0.83	9.8	183	- 70	2.45	21.7
1-dodecanol	112-53-8	6 ± 0.54	186.3	0.83	18.8	258	24	2.48	33.8
Isopropyl myristate	110-27-0	1.4 ± 0.17	270.5	0.85	6.5	315	3	8.48 [b]	51.2
Tributyrin	60-01-5	2.2 ± 0.28	302.4	1.03	8 [c]	307	- 75	1.83	57.4
Decane	124-18-5	0.4 ± 0.05	142.3	0.81	0.84	174	- 29.7	2.21	61.9

All the data are obtained from https://pubchem.ncbi.nlm.nih.gov/ and https://webbook.nist.gov/.
[a] Our experimental data
[b] Data is obtained from *Thermochimica Acta*, 222 (1993) 209-218
[c] Data is obtained from *Bioresources Technology* 56 (1996) 55-60
[d] High purity product from Merck

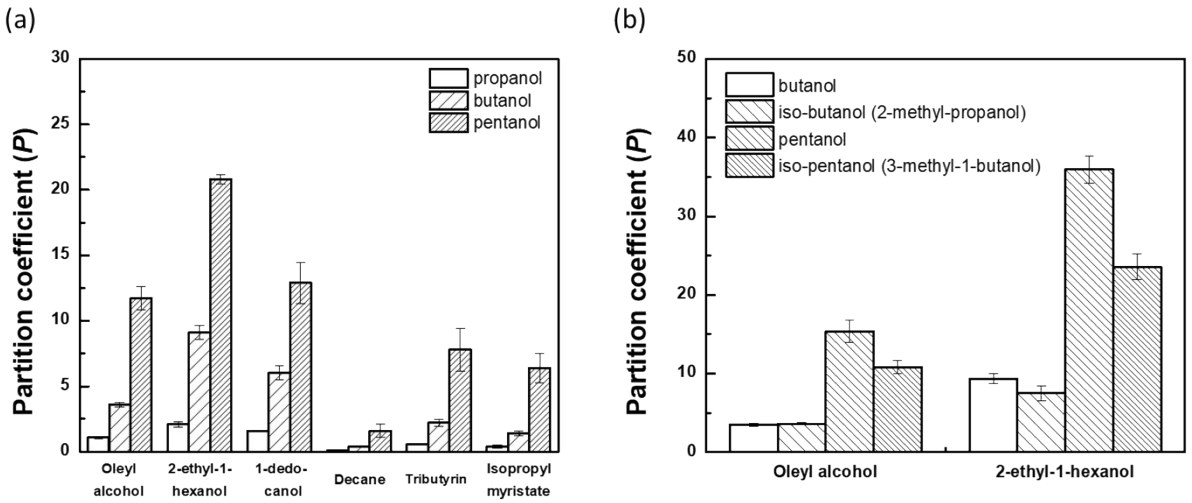

Fig. S2 Partition coefficients of extractants with (a) linear alcohols: n-propanol, n-butanol, and n-propanol and (b) branched alcohols: iso-butanol and iso-pentanol at 37 °C.

S3. Membrane fabrication and information

Three lab-scale thin film composite membranes possessing different separating layers have been fabricated. Depending on the separating layers, different fabrication methods were deployed. All the membranes were crosslinked after membrane fabrication for membrane stability.[24-27]

The porous membrane was fabricated *via* electrospinning (ESR200RDH, NanoNC, South Korea). The hydroxyl polyimide was synthesized through azeotrope imidization with *o*-xylene using three monomers such as 4,4′-oxydiphthalic anhydride, 3,3′-dihydroxy-4,4′-diaminobiphenyl, and 4,4′-oxydianiline. The synthesized hydroxyl polyimide was dissolved in N,N'-dimethylacetamide at 12 *wt*% and spun onto a drum type collector (20 cm x 30 cm) with 15 cm tip to collector distance. After consuming 8 ml dope solution, the nanofibrous membrane was pressed three times at 130 N cm^{-2} for 3 seconds to make the membrane flat and smooth. The pressed membrane was thermally rearranged from hydroxyl polyimide to polybenzoxazole at 400 °C. Then, the final nanofibrous membrane which is chemically and mechanically robust was used as a support layer for other thin film composite membranes. Further details for synthesis and fabrication can be found elsewhere.[24, 28]

The crosslinked polyamide thin film composite membrane was prepared by interfacial polymerization. Two monomer solutions were prepared as a 3.5 *wt*% m-phenyl diamine aqueous solution and a 0.15 *wt*% trimesoyl chloride/hexane solution respectively. The prepared nanofibrous membrane was soaked in an m-phenyl diamine solution for 2 min and after taking out the membrane, the excessive aqueous solution on the surface was removed. Trimesoyl chloride solution was gently poured onto the membrane surface and left for 1 min to react. After polymerization of partially crosslinked polyamide, the thin film composite membrane was washed with pure hexane and then water. Further details for interfacial polymerization and membranes can be found in our previous works.[27]

The crosslinked polydimethylsioxane thin film composite membrane was cast using a gravure coating machine (RK coating, UK). An 8-10% epoxysilicone (ECMS-924, Fluorochem, UK) was mixed with 2 *wt*% photoinitiator (Speedcure 937, Lambson, UK). The mixture was coated onto the membrane surface with a ceramic gravure head engraved 1900 line per inch having a volume capacity of 1 cm^3 m^{-2} at a coating speed less than 7 m min^{-1}. After coating, the membrane was cured by passing through a UV lamp having > 1,000 mJ cm^{-2} (GEW, UK). For this membrane, a different support membrane, which was prepared with a continuous casting machine (Sepratek, South Korea) with Ultem 1000 (Sabic, Saudi Arabia) and PET nonwoven (Hirose, Japan), was used to prevent penetration of the epxysilicone solution during coating. Further details for gravure coating and membranes can be found in our previous work.[25]

The crosslinked sulfonated poly(arylene ether sulfone) thin film composite membrane was fabricated by a spray coating method. The sulfonated polyarylene ether sulfone (Aquafone™, YanJin Technology, China) was dissolved in dimethylsulfoxide with 8 *wt*%. The dope solution was sprayed on the nanofibrous membrane surface using a spray gun (GP-2, Fuso Seiki Co. Ltd, Japan) with 15 cm tip to collector distance and infrared ramp. The temperature on the membrane surface was set at 50 °C. The spray was automatically performed using the electrospinning machine. The nitrogen gas was utilized as a carrier gas at 0.15 bar, and the traverse machine and collector were operated at 325 cm min^{-1} and 780 mm min^{-1} speed. After 0.27 ml m^{-2} loading, the membrane was cured at 180 °C in a convection oven for thermal crosslinking to convert the sulfonic acid group to sulfone linkage. Further information for spray coating method and membranes can be found in our previous work.[26]

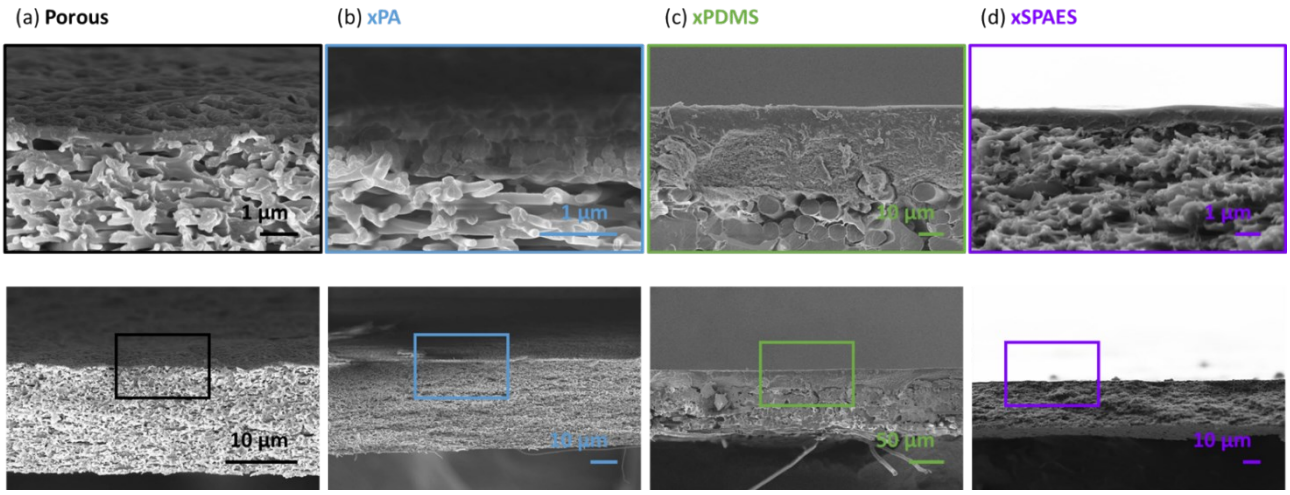

Fig.S3 Cross-sectional SEM images of the fabricated membranes: (a) porous membrane, (b) xPA, (c) xPDMS, and (d) xSPAES. All the samples for the images were prepared by a freeze-fracture method in liquid nitrogen. The prepared samples were dried overnight before coating with 15 nm Cr layer (turbo-molecular pumped coater, Q150TS, Quorum Technologies Ltd., UK). The prepared samples were investigated using Field Emission Gun Scanning Electron Microscope (FEG-SEM, LEO Gemini 1525, Zeiss, Germany) with 8 mm working distance at 10 kV.

A test for phase breakthrough was performed using a crossflow system (**Fig. S4**). Two gear pumps circulated each solution at both sides of a membrane cell (CF016P-FO, Sterlitech, USA). The temperature of both solutions was maintained at 37 °C and the solutions were circulated counter-currently. The system was operated at 1.0 L min^{-1} (0.16 m s^{-1}) circulation rate at each side and less than 1 bar of operating pressure.

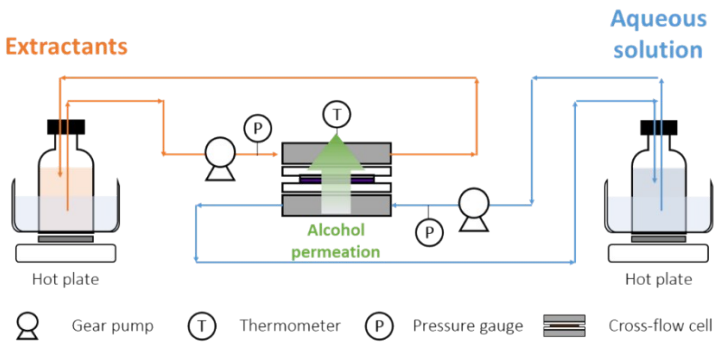

Fig.S4 A perstraction test apparatus for dynamic extraction.

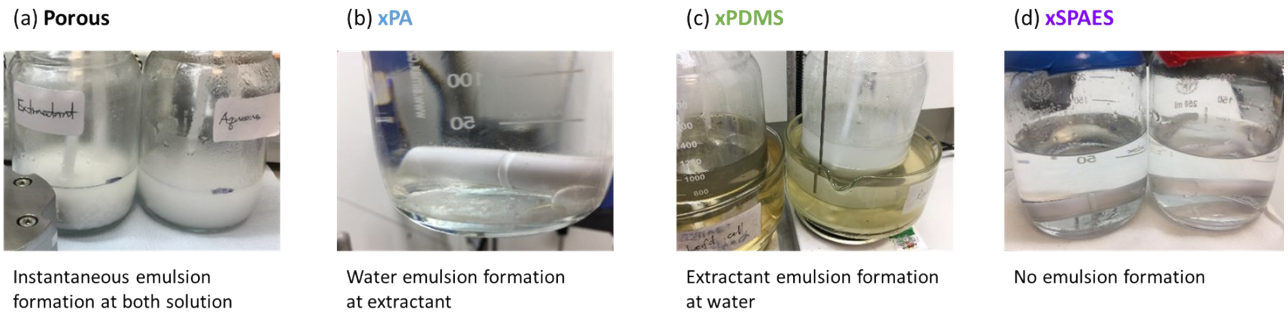

Fig. S5 Digital photographs of emulsion formation with four membranes: (a) porous membrane, (b) xPA, (c) xPDMS, and (d) xSPAES membranes. The tests were performed for not less than 12 h.

Adsorption tests were performed using a quartz crystal microbalance (QCM200, Stanford research systems, UK). Three crystal probes were coated with xSPAES (100.4 ± 15.3 μg) using a spin coating method. 5 ml solution was introduced on the rotating probe at 2,500 rpm and simultaneously irradiated *via* an IR lamp. After preparation, the probes were also crosslinked at 180 °C. The adsorbed amounts of each liquid were measured separately for each probe at 37 °C. The adsorbed amount was calculated by frequency difference following **eqn (S3)**:

$$\Delta f = - C_f \cdot \Delta m \qquad \text{(S3)}$$

where Δf is the observed frequency different in Hz, C_f is the sensitivity factor for crystal (56.6 Hz μg^{-1}), and Δm is the mass difference in g cm^{-2}.

The threshold pressure test was conducted using a dead-end filtration (HP4750 stirred cell, Sterlitech, USA) at 37 °C. The filtration unit was immersed in a water bath maintaining a temperature of 37 °C. The filtration unit was pressurized step-wise from 0.5, 1, 3, 5, 15, and 30 bar with nitrogen gas. Each step was maintained for minimum 6 h. So long as there was no permeation of liquid drops, the pressure was increased further. All the threshold pressures for solvents were determined as pressure, generating a few droplets of liquid permeate for several hours.

S4. Membrane performance

Membrane performance for perstraction was evaluated under both dynamic and steady-state conditions. In the dynamic test, the system concentration varied during operation whilst the system volume remained constant. The dynamic test was performed in the cross-low system (**Fig. S4**), under the same conditions as the phase breakthrough test. In contrast, the steady-state test was performed with dosing pumps adding fresh feed and pure extractant solutions to each system at constant rates so that a steady-state condition is achieved (**Fig. S7**). The concentration of each solution becomes a constant depending on the dosing flow rate when the system reaches steady-state. For investigating membrane permeance and overall mass transfer coefficient, the equation for each system is derived below:[29, 30]

Mass Balance for dynamic test ($dV/dt = 0$) [30]

$$N = V_{Ex}\frac{dC_{Ex}}{dt} = k_{ov} \cdot A \left(PC_{Fe,\,t} - C_{Ex,\,t}\right) \tag{S4}$$

where N is a mass flux (g.s^{-1}) and k_{ov} is an overall mass transfer coefficient of a membrane (m.s^{-1}). P is a partition coefficient. V_{Ex} (m^3) and C_{Ex} (g.L^{-1}) are volume and alcohol concentration of extractant solution. C_{Fe} (g.L^{-1}) is the alcohol concentration of fermentation broth (feed) and A is an effective membrane area (m^2).

$$V_{Fe}\left(C_{Fe,\,0} - C_{Fe,\ t}\right) = V_{Ex}\left(C_{Ex,\,t} - C_{Ex,\,0}\right) \tag{S5}$$

The total mass of extracted alcohol is the same at feed and extractant. Thus, we can derive the **eqn (S4)** as a function of $C_{Ex,\,t}$.

$$V_{Ex}\frac{dC_{Ex}}{dt} = k_{ov} \cdot A \left[P \cdot \left\{C_{Fe,\,0} - \frac{V_{Ex}}{V_{Fe}} \cdot \left(C_{Ex,\,t} - C_{Ex,\,0}\right)\right\} - C_{Ex,\,t}\right] \tag{S6}$$

$$\Big/\left(PC_{Fe,0}+P\frac{V_{Ex}}{V_{Fe}}C_{Ex,0}-(C_{Ex,t}+P\frac{V_{Ex}}{V_{Fe}}C_{Ex,t})\right)dC_{Ex}=\Big/_{V_{Ex}}^{k_{ov}\cdot A}dt \quad \text{(S7)}$$

put $P^{V_{Ex}/V_{Fe}}=\alpha$ and integrates the **eqn (S6)**.

$$(\frac{1}{1+\alpha})\ln\left\{\frac{C_{Ex,0}-PC_{Fe,0}}{(1+\alpha)C_{Ex,t}-PC_{Fe,0}-\alpha C_{Ex,0}}\right\}=\frac{k_{ov}\cdot At}{V_{Ex}} \quad \text{(S8)}$$

Hence, k_{ov} can be obtained from the slope of **eqn (S8)**.

$$J=\Big/_{A}^{N}=\frac{V_{Ex}dC_{Ex}}{A\quad dt}=\frac{V_{Ex}C_{Ex,t}-C_{Ex,0}}{A\qquad t}=k_{ov}(PC_{Fe,t}-C_{Ex,t}) \quad \text{(S9)}$$

where J is a alcohol permeance (g.m^{-2}.h^{-1}).

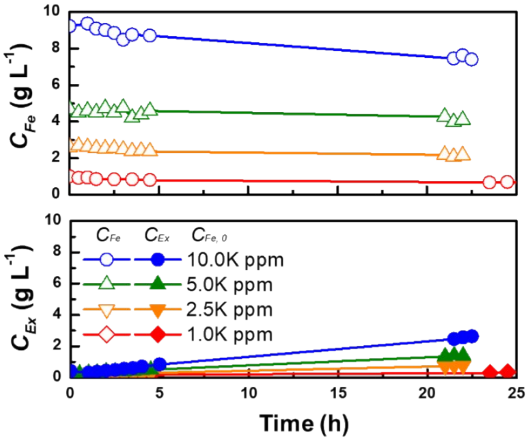

Fig. S6 The butanol concentration profiles at feed and extractant which were tested using xSPAES with 1 L of different feed solutions (0.1, 0.25, 0.5, and 1.0 g L^{-1} aqueous solution) and pure 2EH, respectively.

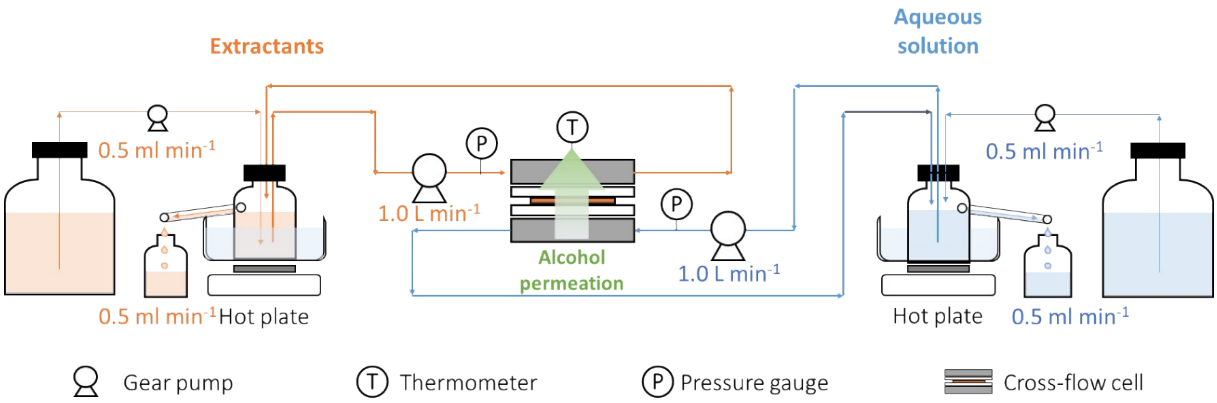

Fig. S7 Perstraction test apparatus for steady-state extraction

The steady-state experiments were performed with two additional HPLC pumps dosing each solution (fresh feed and pure extractant) into each flask at 0.5 ml min^{-1} (**Fig. S7**). Each flask has an overflow stream at the same flowrate as the dosing solutions. The other components were the same as in the dynamic test except for the test volume. Each feed and extractant flask has 100 ml volume with a magnetic stirrer. Therefore, when each system reaches constant concentration ($dC/dt = 0$), one can calculate an overall mass transfer coefficient and flux at steady-state following **eqn (S14)** below. Samples for concentration measurements were taken from each flask over time. The equations for permeance and overall mass transfer coefficient were derived below:

Mass Balance for steady state test ($dC/dt = 0$) [29]

$$N = C_{Ex}\frac{dV_{Ex}}{dt} = C_{Ex}F_{Ex} = k_{ov} \cdot A\left(PC_{Fe} - C_{Ex}\right) \tag{S10}$$

$$C_{Ex}F_{Ex} = C_{Fe}F_{Fe} \tag{S11}$$

where the concentrations at both solutions (C_{Ex} and C_{Fe}) are constant. F is a flow rate of dosing pump at each solution (ml min^{-1}).

$$N = C_{Ex}\frac{dV_{Ex}}{dt} = C_{Ex}F_{Ex} = k_{ov} \cdot A\left(P\frac{F_{Fe}}{F_{Ex}}C_{Ex} - C_{Ex}\right) \tag{S12}$$

$$P\frac{\dot{F}_{Fe}}{\dot{F}_{Ex}} = \beta$$

put

$$k_{ov} = {\dot{F}_{Ex}}/{A(\beta - 1)} \quad \text{(S13)}$$

$$\dot{J} = {\dot{N}}/{A} = \frac{C_{Ex}}{A}\dot{F}_{Ex} = k_{ov} \cdot (PC_{Fe} - C_{Ex}) \quad \text{(S14)}$$

where $\dot{J}$ is a alcohol permeance (g.m^{-2}.h^{-1}).

The diffusivity of A into B (D_{AB}) is calculated by **eqn (S15)**:[31]

$$D_{AB} = \frac{7.4 \times 10^{-8}(\emptyset_B \cdot M_B)^{1/2} \cdot T}{\mu_B \cdot V_A^{0.6}} \quad \text{(S15)}$$

where Φ is an association factor of liquid B (2.26 for water and 1 for organic solvents), M_B is a molecular weight of liquid , T is a temperature, μ_B is a dynamic viscosity of liquid B, and V_A is a molar volume of solute A.

The mass transfer coefficient of liquid film 'i' is calculated by following **eqn (S16)**:

$$k_i = \frac{Sh \cdot D_s}{d_h} = 1.62 \cdot \left(Re \cdot Sc \cdot \frac{d_h}{L_c}\right)^{\frac{1}{3}} \frac{D_s}{d_h} = 1.62 \cdot \left(\frac{v \cdot D_s^2}{d_h \cdot L_c}\right)^{1/3} \quad \text{(S16)}$$

where Sh, Re, and Sc are Sherwood, Reynolds, and Schimidt numbers, respectively; d_h is a hydraulic diameter, D_S is a solute diffusivity to solvent 'i', Lc is a channel length of the membrane cell, v is a mean velocity of solvent 'i'.

The overall mass transfer resistance was investigated into three parts following resistances-in-series model **(Fig. S8)**. Contributions of each resistance '*i*' (γ_i) were calculated following **eqns (S17) – (S19)**.

$$\gamma_{Fe} = \left[\frac{P}{k_{Fe}} \Big/ \frac{1}{k_{ov}}\right] \times 100 = \left[\frac{P}{k_{Fe}} \Big/ \left(\frac{P}{k_{Fe}} + \frac{1}{k_m} + \frac{1}{k_{Ex}}\right)\right] \times 100 \quad \text{(S17)}$$

$$\gamma_m = \left[\frac{1}{k_m} \Big/ \frac{1}{k_{ov}}\right] \times 100 = \left[\frac{1}{k_m} \Big/ \left(\frac{P}{k_{Fe}} + \frac{1}{k_m} + \frac{1}{k_{Ex}}\right)\right] \times 100 \quad \text{(S18)}$$

$$\gamma_{Ex} = \left[\frac{1}{k_{Ex}} \Big/ \frac{1}{k_{ov}}\right] \times 100 = \left[\frac{1}{k_{Ex}} \Big/ \left(\frac{P}{k_{Fe}} + \frac{1}{k_m} + \frac{1}{k_{Ex}}\right)\right] \times 100 \quad \text{(S19)}$$

where k_{aq}, k_m, and k_{Ex} are mass transfer coefficients of feed, membrane, and extractant, respectively.

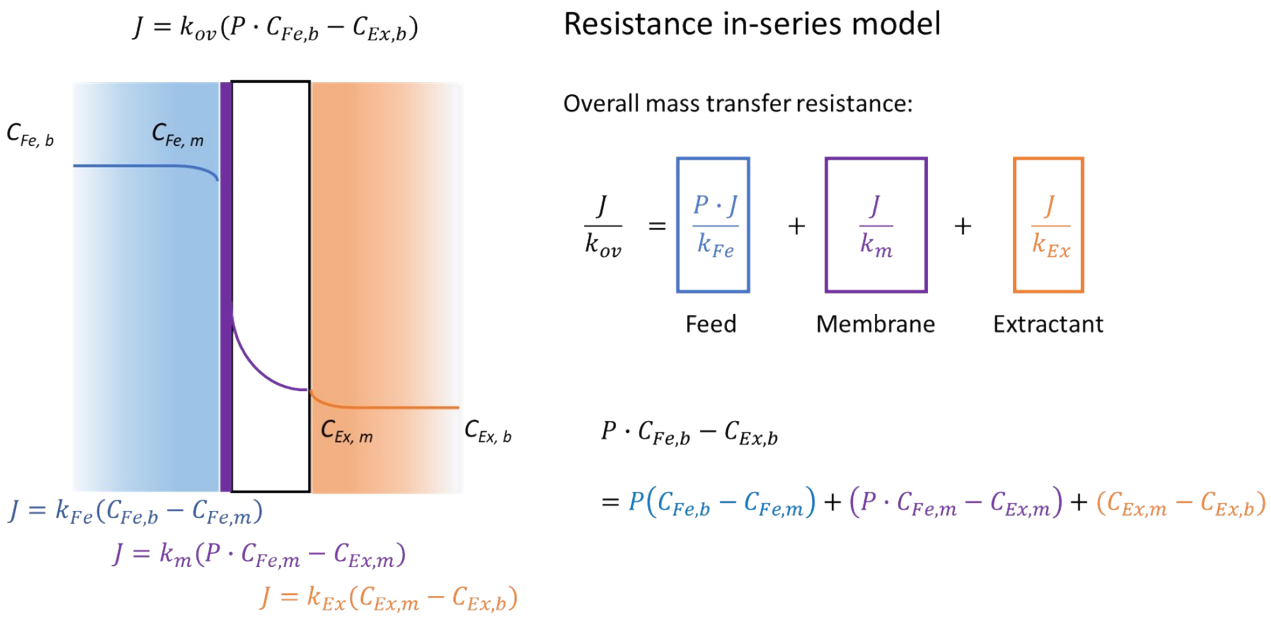

Fig. S8 Schematic diagram of a resistances-in-series model for perstraction. The overall mass transfer coefficient consists of three parts: two liquid films (feed and extractant) and a membrane. The membrane is placed facing the feed to prevent fouling and pore clogging on the porous support. $C_{Fe,b}$ and $C_{Fe,m}$ are concentrations at bulk feed and membrane surface on feed side at equilibrium state. $C_{Ex,b}$ and $C_{Ex,m}$ are concentrations at bulk extraction and membrane surface on extractant side.

Mass transfer coefficients of liquid films were calculated by **eqns (S15) and (S16)**. The mass transfer coefficient of the membrane was calculated from **eqn (3)**. Depending on target alcohols, contributions of each part were summarized in **Table S6**.

Table S6 Mass transfer coefficients and contributions of liquid films (feed and extractant) and membrane to the overall mass transfer coefficient.

	k_{ov} (m s^{-1})	k_{Fe} (m s^{-1})	k_{Ex} (m s^{-1})	k_m (m s^{-1})	γ_{Fe} (%)	γ_{Ex} (%)	γ_m (%)
n-PrOH	5.0E-07*	7.4E-06	2.8E-06	7.6.E-07	3.0	20.7	76.3
n-BuOH	5.0E-07*	6.8E-06	2.6E-06	6.8.E-07	7.1	19.2	73.6
n-PnOH	3.0E-07	6.8E-06	2.5E-06	3.7.E-07	6.9	12.0	81.1

* The exact values of mass transfer coefficient for n-PrOH and n-BuOH were found to be 0.47E-06 and 0.48E-06, respectively. The values were rounded to 1 significant figure since the dosing flowrate, F_{Ex} (eqn (2)), was controlled at 0.5 ml min^{-1} from available increments of 0.1 ml min^{-1} which determines the number of significant figures in the calculation.

S5. Theoretical study for effects of extractant/feed volume ratio on the process

The theoretical calculations for energy consumption of the continuous biofuel production with perstraction were performed based on four assumptions:(i) a fixed feed solution (10 L 1*wt*% n-$BuOH_{aq}$); (ii) a fixed overall mass transfer coefficient (5.0 x 10^{-7} m s^{-1}) and membrane area (1 m^2); (iii) initial and saturated extractant concentrations ($C_{Ex,0}$= 0 and

$C_{Ex,t}^{RF} = recovery\ factor \times {}^{C_{Fe,0} \cdot P}\Big/(1 + P \cdot \frac{V_{Ex}}{V_{Fe}})$, *recovery factor* = 0.1, 0.3, 0.5, and 0.99), and; (iv) extractant is recycled after distillation. The continuous biofuel production system was employed at steady state (**Fig. S9**). The mass rate of butanol is the same at three components: fermentation broth (production rate), perstraction (extraction rate), and distillation (distillation rate). The recovery rate and process time at each volume ratio and recovery factor were calculated based on **eqn (S6)** with $C_{Ex,0}$ and $C_{Ex,t}^{RF}$. The recovery factor indicates that the concentration of butanol in extractant is maintained below the saturation concentration of extractant for that level of recovery factor. High recovery factor (0.99) is close to the saturation level of extractant therefore butanol is obtained with less energy consumption for distillation compared to low recovery factor. However, the trade-off is in the recovery rate which dramatically decreases resulting in long process time per unit kg of butanol production. In **Fig. S10a**, the recovery rate decreases when volume ratio increases. Furthermore, the high recovery factor ($high\ RF\ at\ C_{Ex,t}^{RF}$) showed dramatic changes in the recovery rate as following **eqn (S6)** from $C_{Ex,0}$ to $C_{Ex,t}^{RF}$. However, mass flow of the recovered butanol (dw_{Ex}/dt) is the same regardless volume ratio (V_{Ex}/V_{Fe}) (**Fig. S10b**). Therefore, the process time per unit kg of butanol production is correlated to recovery factor (**Fig. S10c**). The energy consumption at all conditions were calculated using Aspen RadFrac distillation from NRTL (Non-Random Two Liquid) model of Aspen Plus v8.4, as described in **Section S1**. In **Fig. S10d**, the energy consumptions were plotted with process time to produce unit kg of butanol. The optimum point can be found with the smallest area between the point and origin. All the simulation results were tabulated in **Table S7**.

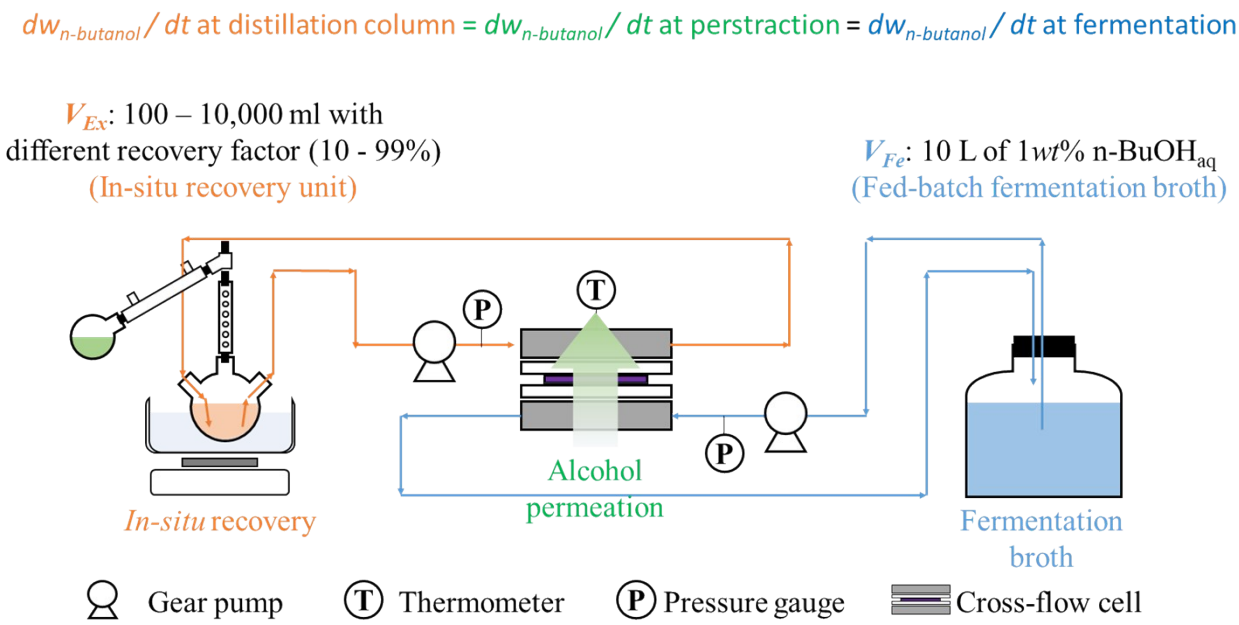

Fig. S9 Schematic diagram of the continuous butanol production system at steady state. The mass flow of butanol at fermentation broth, perstraction, and distillation is the same. The alcohol concentration in the fermentation broth is maintained at 1 *wt*% by producing alcohol at the same rate with the extraction and distillation. The extractant after distillation is recycled and all the extracted alcohol is recovered in the condenser.

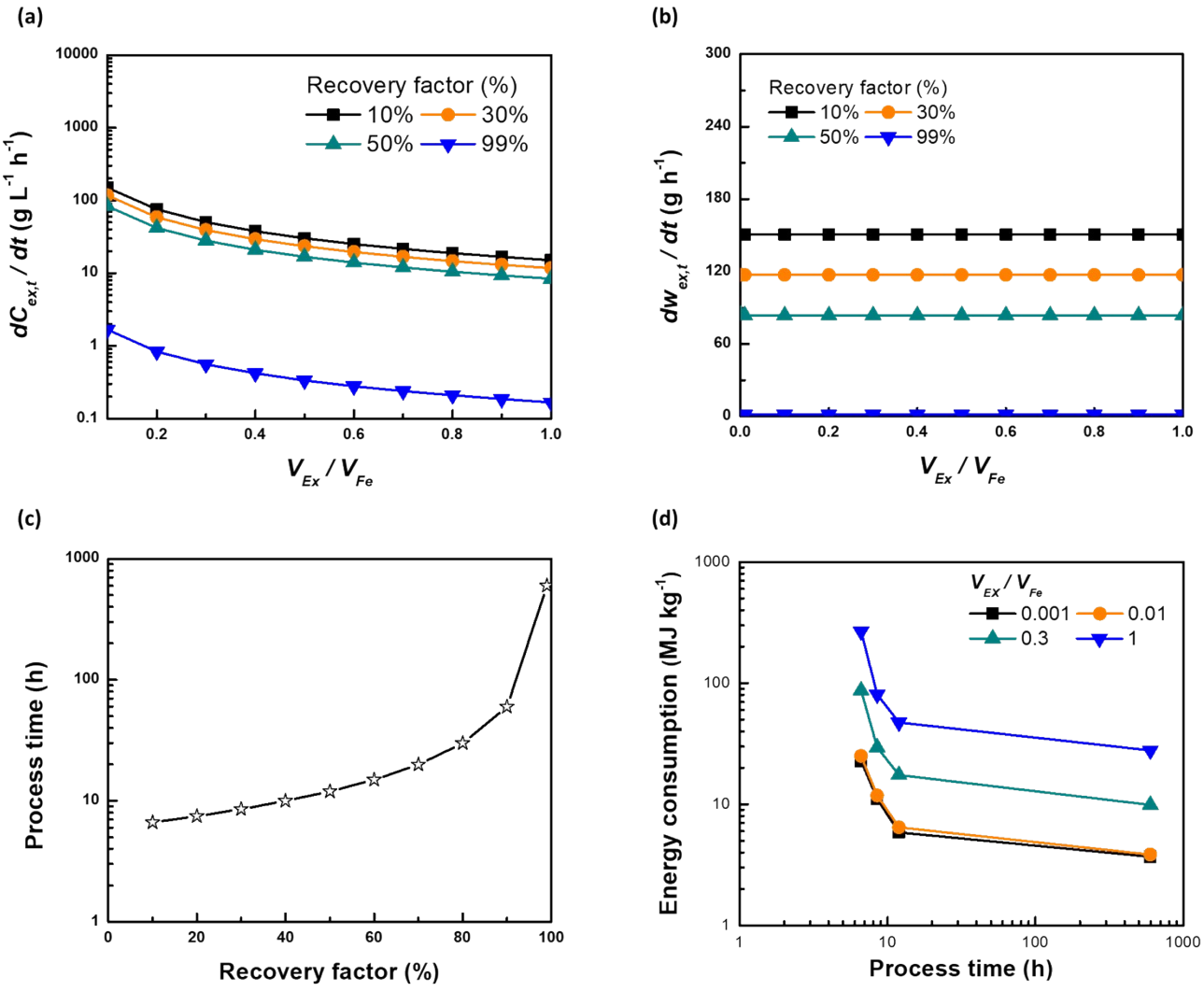

Fig. S10 Recovery rate in (a) concentration ($^{dC_{Ex}/dt}$, g L^{-1} h^{-1}) and (b) mass ($^{dw_{Ex}/dt}$, g h^{-1}) of butanol at extractant were plotted at different volume ratio of extractant:feed ($^{V_{Ex}/V_{Fe}}$) with varying recovery factors (%). (c) Process time (h kg^{-1}) was calculated using the mass rate to produce unit kg of butanol. (d) Energy consumption per unit kg of butanol production was calculated at different volume ratio ($^{V_{Ex}/V_{Fe}}$) and recovery factor (%) which is corresponded to process time (h kg^{-1}).

Table S7 Simulation results for energy consumption at different volume ratio of extractant:feed (V_{Ex}/V_{Fe}) and recovery factor. The specific energy was calculated by dividing the total duty by mass flow. The details for Aspen simulation are described in **Section S1**. The blue column is the optimum condition for the continuous perstraction system in this simulation. The red column represents the optimum condition for batch system.

	Recovery factor	0.1				0.3			
Feed stream	V_{Ex}/V_{Fe}	0.001	0.01	0.3	1.0	0.001	0.01	0.3	1.0
	V_{ex} (L)	0.01	0.1	3	10	0.01	0.1	3	10
	Feed concentration (g L^{-1})	9.2	8.5	2.5	0.9	27.6	25.5	7.4	2.7
	Feed stream rate (L h^{-1})	16.35	17.71	61.40	166.86	4.24	4.59	15.92	43.26
Distillation Column	Distillate to feed (mol%)	0.0187	0.0179	0.0052	0.0019	0.0573	0.0530	0.0155	0.0057
	Reflux ratio	1.2	2.2	10.0	50.0	2.5	2.7	3.0	10.0
	Distillate rate (g h^{-1})	144.4	149.4	149.7	149.1	116.28	116.16	116.1	116.0
	Distillation column temperature (^oC)	52.67				52.67			
	Reboiler temperature (^oC)	104.5				104.5			
	n-butanol purity from distillate (*wt*%)	99.6	99.6	99.5	99.5	99.8	99.8	99.7	99.7
Duty	Reboiler (kJ h^{-1})	3057.38	3404.51	11864.10	34425.20	1000.85	1078.02	3087.43	8435.68
	Condenser (kJ h^{-1})	-217.34	-326.94	-1126.00	-5197.51	-278.08	-293.62	-317.43	-871.98
Total	Specific butanol production energy (MJ kg^{-1})	22.77	25.08	87.20	267.08	11.02	11.83	29.41	80.49
	Required energy and time (MJ h kg^{-2})	151.14	166.47	578.79	1772.73	94.04	100.96	250.98	686.89

	Recovery factor	0.5				0.99			
Feed stream	V_{Ex}/V_{Fe}	0.001	0.01	0.3	1.0	0.001	0.01	0.3	1.0
	V_{ex} (L)	0.01	0.1	3	10	0.01	0.1	3	10
	Feed concentration (g L^{-1})	0.0569	0.0525	0.0151	0.0056	0.1126	0.1040	0.0300	0.0110
	Feed stream rate (L h^{-1})	1.82	1.97	6.80	18.54	0.0184	0.0199	0.0689	0.1873
Distillation Column	Distillate to feed (mol%)	0.0939	0.0870	0.02577	0.0095	0.1791	0.1664	0.0505	0.0188
	Reflux ratio	0.6	0.8	1.3	5.0	0.4	0.4	1.0	5.0
	Distillate rate (g h^{-1})	83.0	83.0	82.7	83.0	1.66	1.66	1.7	1.7
	Distillation column temperature (°C)	52.67				52.67			
	Reboiler temperature (°C)	104.5				104.5			
	n-butanol purity from distillate (*wt*%)	99.6	99.7	99.6	99.6	99.6	99.7	99.7	99.7
Duty	Reboiler (kJ h^{-1})	394.52	432.37	1307.20	3576.02	4.51	4.77	14.05	39.35
	Condenser (kJ h^{-1})	-90.82	-102.15	-129.97	-340.36	-1.59	-1.58	-2.27	-6.81
Total	Specific butanol production energy (MJ kg^{-1})	5.87	6.46	17.46	47.38	3.69	3.85	9.87	27.84
	Required energy and time (MJ h kg^{-1})	70.13	77.18	208.60	566.07	2204.30	2299.88	5896.06	16630.82

S6. Fermentation of Clostridium acetobutylicum ATCC 824

The anaerobic fermentation was conducted following Nature Protocol.[32] The micro-organism was purchased from ATCC (USA) and grown in a Hungate tube and fermentator for cell propagation and fermentation, respectively. The whole procedure can be seen in **Appendix S5**. All the equipment and growth medium were autoclaved at 180 °C (K360s, Touchclave-lab, LTE Scientific, UK). All experiments were performed under anaerobic conditions. 0.5 ml of micro-organisms was precultured in a Hungate tube with 10 ml clostridium growth medium for 1 day until optical density at 600 nm ($O.D._{600}$) reaches 1 – 2.0. Subsequently, 4 ml of the growth medium were transferred to 100 ml of the fresh growth medium and incubated until $O.D._{600}$ reached 1.0 – 2.0. Following the protocol, when $O.D._{600}$ was higher than 0.5, the medium was diluted with deionized water to measure accordingly. When measuring the alcohol concentration, micro-organisms in the samples were separated by centrifuge (13,000 rpm with Micro Centaur, MSE Ltd, UK) and filter (0.45 μm) prior to gas chromatography analysis. 50 ml of the prepared 100 ml inoculum was poured into the fermenter with 750 ml deionized water and 200 ml concentrated growth medium under purging with anaerobic gas (200 ml min^{-1}). The broth was stirred with an overhead stirrer at 200 rpm and adjusted firstly at pH 5.8 using 20 *wt*% phosphoric acid aqueous solution *via* a peristaltic pump. After 6 h fermentation, the pH was adjusted and maintained to be higher than 5.0 by slow addition of 5 M KOH aqueous solution using a peristaltic pump.

In this study, to standardize the tests, the fermentation was terminated once the $O.D._{600}$ reached 8.0. The broth was distributed in different flasks exposed to air and $n\text{-}BuOH_{aq}$ concentration was adjusted to 1.0 *wt*% after checking the concentration of each solution. The partition coefficients of acetone and ethanol which can also be produced during fermentation into 2-ethyl-1-hexanol are extremely low at 0.07 ± 0.021 and 2.8 ± 0.33 respectively, as compared to n-butanol (9.3). Therefore, the acetone and ethanol concentrations were ignored in the test broth.

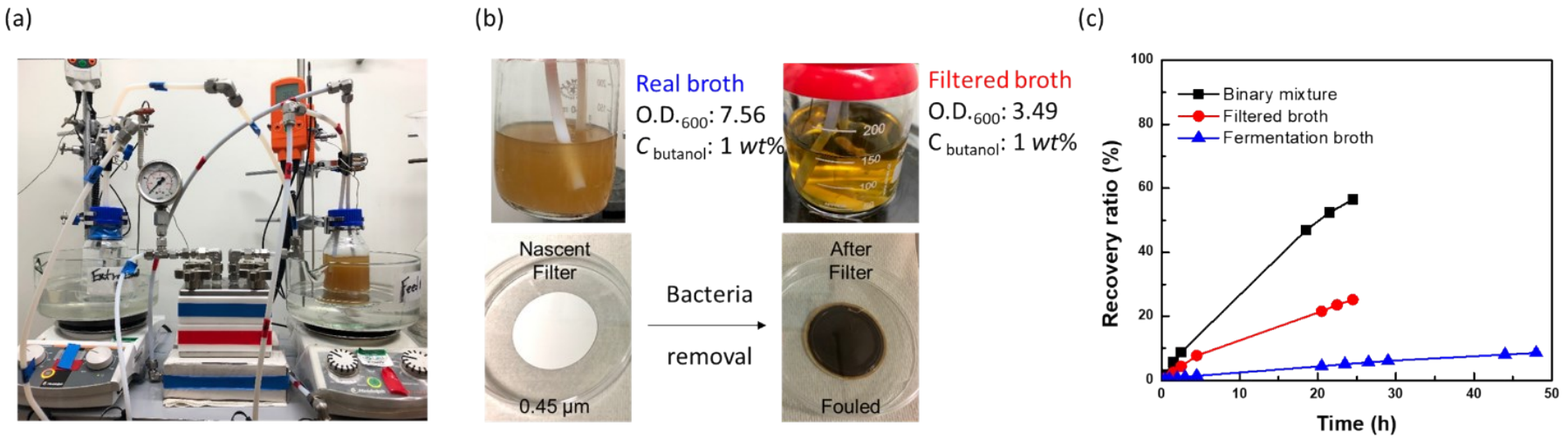

Fig. S11 (a) a dynamic test apparatus for a perstraction system with real fermentation broth, (b) digital photographs of real broth and filtered broth through a 0.45 μm filter, (c) the recovery rate of xSPAES with different feed solutions such as binary mixture, filtered broth and fermentation broth.

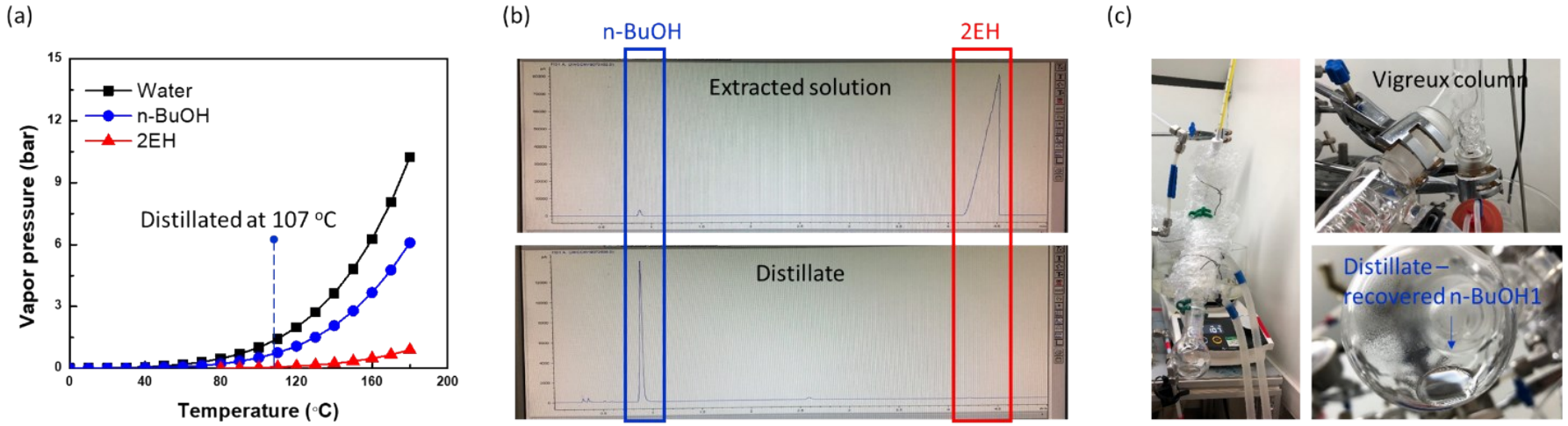

Fig. S12 (a) vapor pressure of water, n-BuOH, and 2EH, (b) digital photographs of gas chromatograph profile of feed solution and distillate, and (c) lab-scale distillation system with a vigreux column and distillated n-BuOH from the extractant.

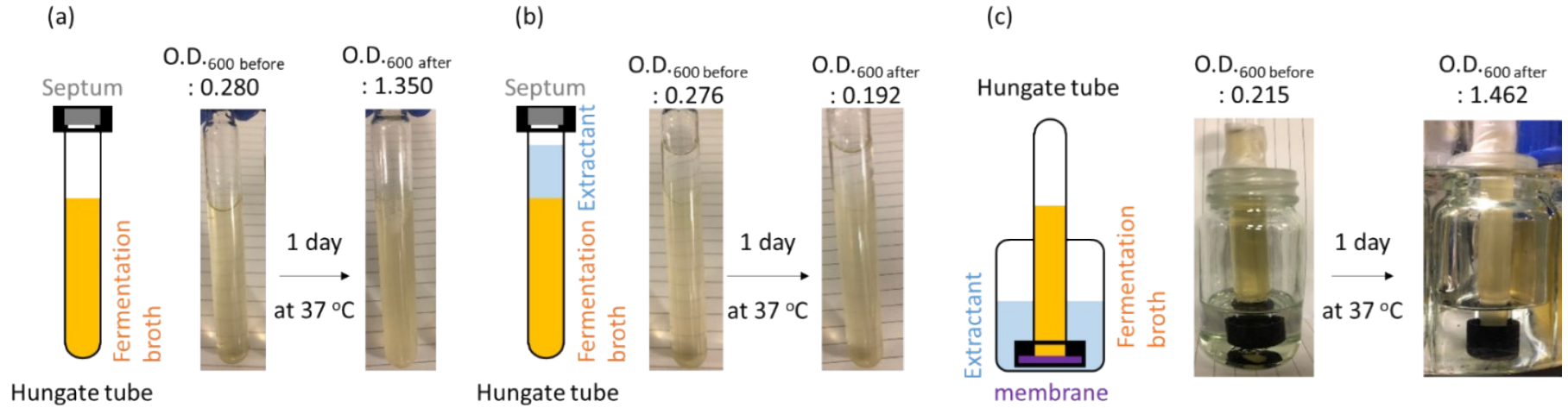

Fig. S13 Propagation of Clostridium acetobutyricum (ATCC 824) in Hungate tube under anaerobic conditions (a) without extractant (as a control) and (b) with extractant (2EH as an inhibitor) and (c) protecting with xSPAES instead of butyl rubber septum. Optical density at 600 nm ($O.D._{600}$) was measured before and after one-day incubation at 37 °C.

Appendix S1. Potential separations by membrane-based extraction (perstraction) in literature [15, 31, 33-37]

Terminology	Membrane type	Application	Year	Reference	No. Reference
Perstraction	Cellulose acetate or polyvinylchloride	Liquid mixture separation using perstraction and pervaporation	1973	US3933647A (Fritz Muller)	33
	Rayon	Elimination of ethanol inhibition	1986	Biotechnol. Bioeng., 28, 534	34
	Polydimethyl phenylene oxide	Separation of liquid benzene/cyclohexane mixture	1988	J. Membr. Sci., 37, 205	35
	Polyurea-urethane	Separation of multiring aromatic hydrocarbons	1990	US4962271A (ExxonMobil)	36
	Cellulose acetate	Crude reaction product from a metal catalyst	1993	US5298669A (ExxonMobil)	37
	Silicon rubber membrane	Citronellol and geraniol separation	2008	J. Membr. Sci., 317, 50	31
	PDMS membrane with ionic liquids	ABE fermentation	2017	J. Membr. Sci., 537, 337	15

Appendix S2. Partition coefficient measurement

Partition coefficient measurement

1. To prepare homogeneous 50 ml of 5000 ppm of alcohol / aqueous or extractants solutions. *
2. To mix two solutions vigorously.
3. To keep the mixture to reach an equilibrium state at 37 °C. (for 24 h)
4. To analyze the concentration of separated each solution through G.C.

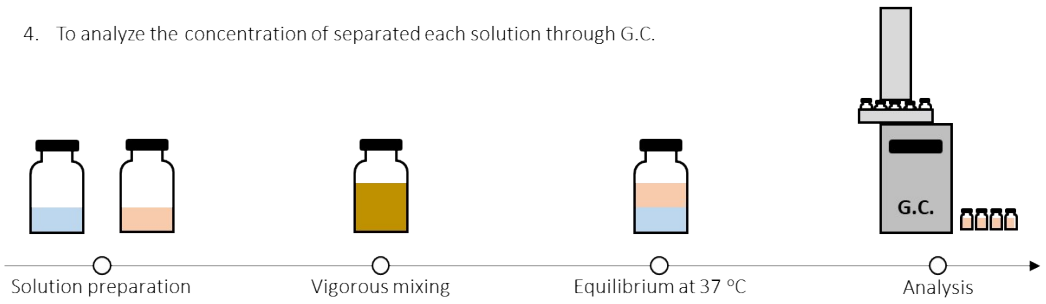

* The alcohol concentration of fermentation broth is below than 1 *wt*% alcohol in the fermentation broth (10,000 ppm). Each standard curve of alcohol concentration in each solvent has been prepared.

Appendix S3. Gas chromatography measurement

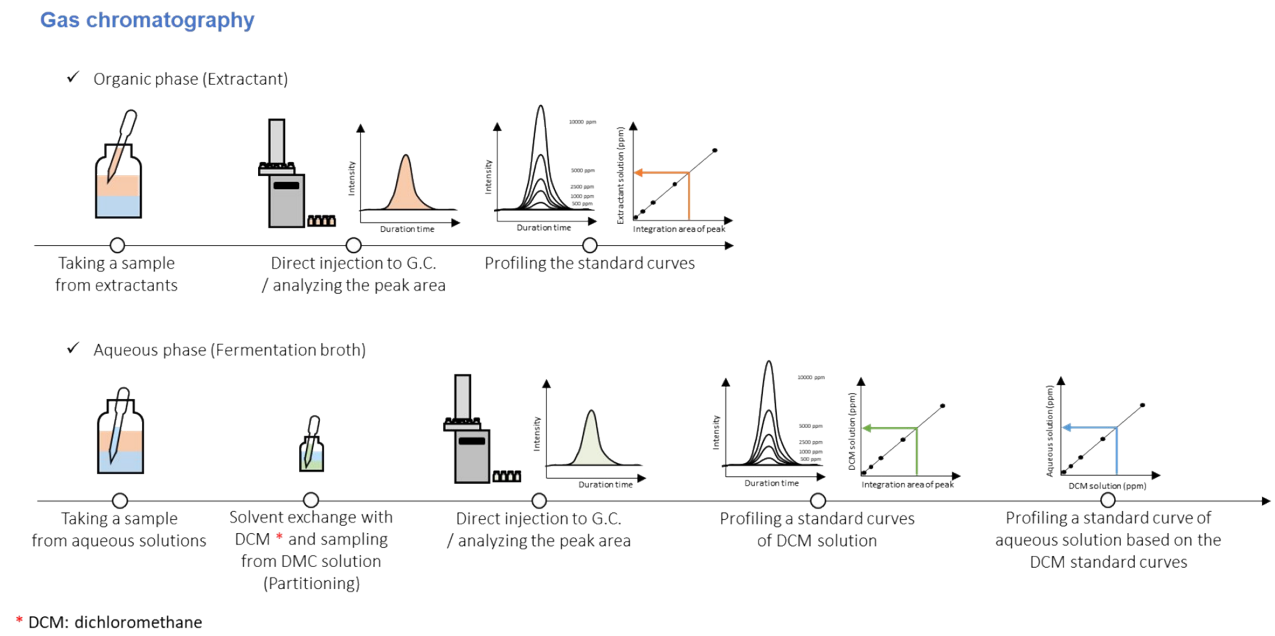

* DCM: dichloromethane

Appendix S4. Standard curves

	Extractant	Aqueous solution
n-PrOH	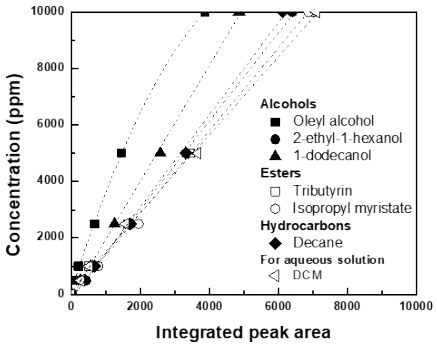	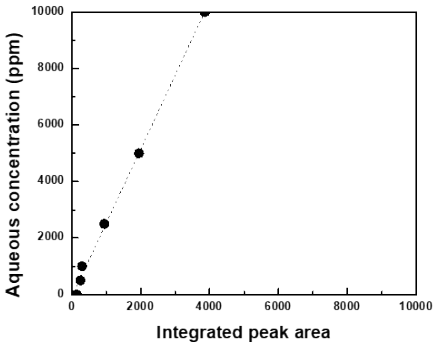
n-BuOH	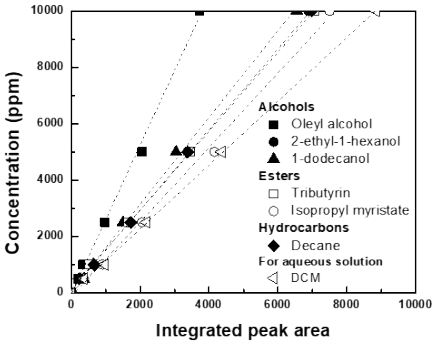	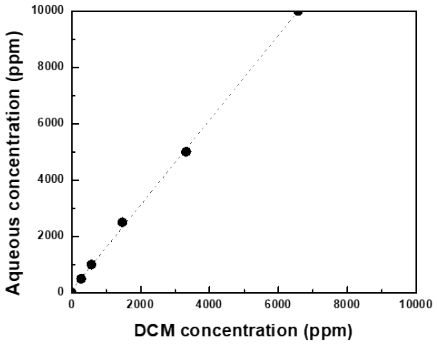
n-PnOH	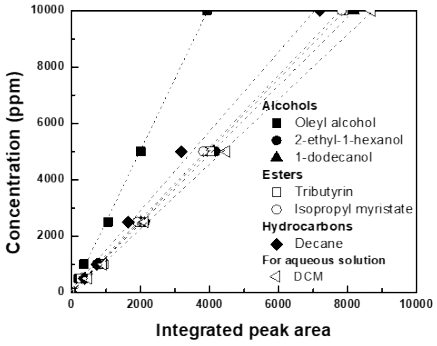	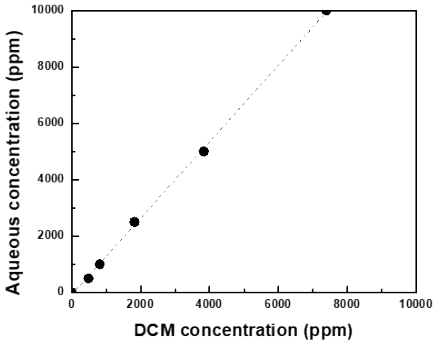

Linear and polynomial fittings by OriginPro 8.5

		n-PrOH		n-BuOH		n-PnOH	
Extractants	Oleyl alcohol	$y = -3E\text{-}04\ x^2 + 3.7868\ x + 168.04$	0.999	$y = 2.6431\ x - 40.839$	0.997	$y = 2.539\ x - 29.592$	0.999
	2-ethyl-1-hexanol	$y = 1.5627\ x - 107.33$	0.999	$y = 1.4469\ x + 60.871$	0.999	$y = 1.2478\ x - 37.361$	0.999
	1-dodecanol	$y = 2.0527\ x - 82.558$	0.999	$y = 1.9093\ x + 97.494$	0.999	$y = 1.2192\ x + 17.992$	1.000
	Decane	$y = 1.63\ x - 146.64$	0.998	$y = 1.4258\ x + 91.487$	0.999	$y = 1.4052\ x + 94.265$	0.996
	Tributyrin	$y = 1.4193\ x + 61.892$	0.999	$y = 1.4026\ x + 136.47$	0.997	$y = 1.2622\ x - 4.5776$	0.999
	Isopropyl myristate	$y = 1.4665\ x – 61.56$	0.998	$y = 1.3207\ x - 128.37$	0.999	$y = 1.2787\ x + 32.058$	0.999
	DCM	$y = 1.3789\ x + 144.42$	0.999	$y = 1.1426\ x - 4.4468$	0.999	$y = 1.3649\ x – 9.6435$	0.998
Aqueous solution		$y = 2.6152\ x - 81.877$	0.997	$y = 1.5050 + 106.3405$	0.999	$y = 1.3562\ x – 75.6553$	0.999

The integrated peak areas of the main extractants and aqueous solution

n-PrOH	Oleyl alcohol	2-ethylhexanol	Aqueous solution
500 ppm	49.7	423.4	250.2
1,000 ppm	203.7	655.8	297.2
2,500 ppm	672.1	1720.1	946.5
5,000 ppm	1450.2	3364.9	1950.2
10,000 ppm	3872.2	6406.4	3864.4

n-BuOH	Oleyl alcohol	2-ethylhexanol	Aqueous solution
500 ppm	194.9	279.8	274.0
1,000 ppm	338.0	647.5	570.7
2,500 ppm	975.0	1690.0	1468.5
5,000 ppm	2052.8	3372.4	3318.6
10,000 ppm	3720.5	6889.7	6568.6

n-PnOH	Oleyl alcohol	2-ethylhexanol	Aqueous solution
500 ppm	205.9	331.7	485.1
1,000 ppm	358.3	820.0	807.4
2,500 ppm	1056.9	2128.4	1820.8
5,000 ppm	2007.1	4174.5	3837.1
10,000 ppm	3924.9	7951.5	7394.0

Appendix S5. Fermentation with clostridium acetobutylicum (ATCC 824)

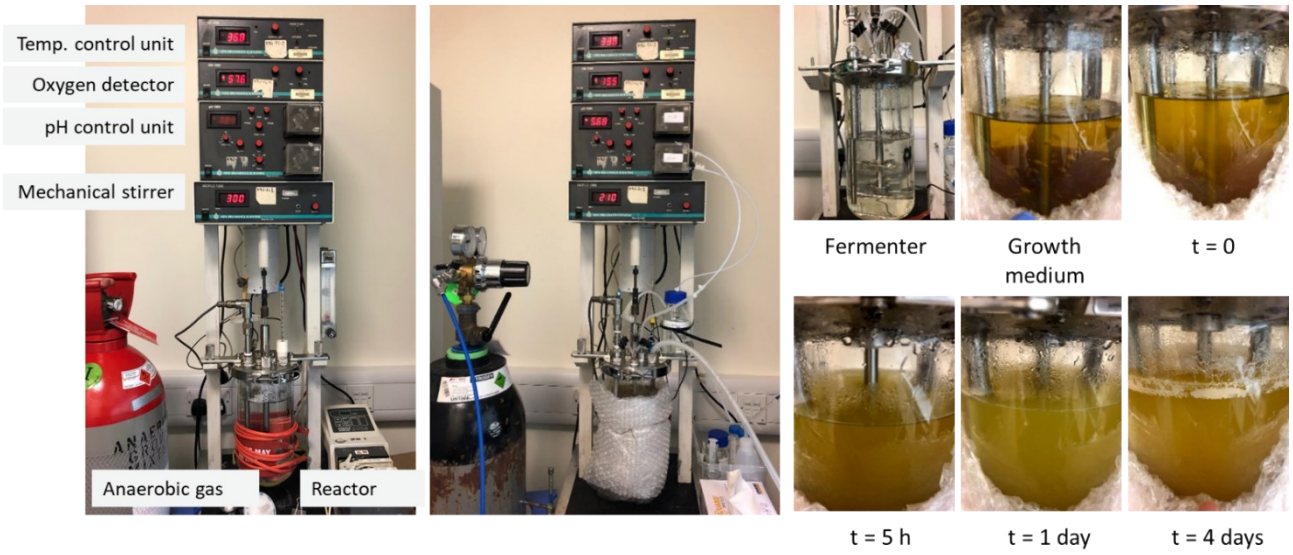

List of Symbols and abbreviations

Symbol		Symbol	
α_{ab}	Selectivity	A	The effective membrane area (m^2)
y_a	Fractional ratio of 'a' in permeate	$C_{Ex,t}$	Alcohol concentration of extractant at time 't' (g L^{-1})
x_a	Fractional ratio of 'a' in feed	$C_{Ex,0}$	Alcohol concentration of extractant at time '0' (g L^{-1})
Δf	The frequency difference in quartz microbalance in Hz	$C_{Ex,b}$	Alcohol concentration at bulk extractant (g L^{-1})
C_f	The sensitivity factor of crystal for quartz microbalnce (56.6 Hz μg^{-1})	$C_{Ex,m}$	Alcohol concentration at membrane surface of extractant side (g L^{-1})
Δm	The mass difference in auqrtz microbalance (g cm^{-2})	$C_{Fe,t}$	Alcohol concentration of feed at time 't' (g L^{-1})
J	Alcohol permeance (g $m^{-2} h^{-1}$)	$C_{Fe,0}$	Alcohol concentration of feed at time '0' (g L^{-1})
$\dot{N}$	Mass flux (g s^{-1})	$C_{Fe,b}$	Alcohol concentration at bulk feed (g L^{-1})
V_{Ex}	Volume of extractant solution (m^3)	$C_{Fe,m}$	Alcohol concentration at membrane surface of feed side (g L^{-1})
V_{Fe}	Volume of feed solution (m^3)	$\dot{F_{Ex}}$	Flow rate of dosing pump at extractant (ml min^{-1})
k_{ov}	The overall mass transfer coefficient (m s^{-1})	$\dot{F_{Fe}}$	Flow rate of dosing pump at feed solution (ml min^{-1})
k_{Fe}	The mass transfer coefficient at feed (m s^{-1})	D_{AB}	Diffusivity of A into B (cm^2 s^{-1})
k_{Ex}	The mass transfer coefficient at extractant (m s^{-1})	$\emptyset_B$	Association factor of liquid B (2.26 for water and 1 for organic solvents)
k_m	The mass transfer coefficient at membrane (m s^{-1})		
P	Partition coefficient		

Symbol		Abbreviation	
M_B	Molecular weight of liquid B (g mol^{-1})	PS	Perstraction
T	Temperature (K)	LL	Liquid-liquid extraction
μ_B	Dynamic viscosity of liquid B (cP)	GS	Gas stripping
V_A	Molar volume of solute A (m^3 kg^{-1} mol^{-1})	PV	Pervaporation
Sh	Sherwood number	2EH	2-ethyl-1-hexanol
Re	Reynolds number	OA	Oleyl alcohol
Sc	Schmidt number	xPA	Crosslinked polyamide
d_h	Hydraulic diameter (m)	xPDMS	Crosslinked polydimethylsiloxane
Lc	Channel length of the membrane cell (m)	xSPAES	Crosslinked sulfonated polyarylene ether sulfone
v	Mean linear velocity of solvent (m s^{-1})	QCM	Quartz crystal microbalance
γ_{Fe}	Adverse contribution of feed liquid film on performance (%)	n-BuOH	n-butanol
γ_{Ex}	Adverse contribution of extractant liquid film on performance (%)	n-PrOH	n-propanol
γ_m	Adverse contribution of membrane liquid film on performance (%)	n-PnOH	n-pentanol
δ	Solubility parameter ($MPa^{-1/2}$)	RR	Recovery ratio
		RF	Recovery factor
		FEG-SEM	Field Emission Gun Scanning electron microscopy
		$O.D._{600}$	Optical density at 600 nm
		TFC	Thin-film composite

References

1. V. B. M, M. M. K and A. P. R. G, *Renew. Sust. Energ. Rev.*, 2017, **78**, 1068-1088.
2. S. Atsumi, T. Hanai and J. C. Liao, *Nature*, 2008, **451**, 86-89.
3. H. E. Murdock, D. Gibb, T. André, F. Appavou, A. Brown, B. Epp, B. Kondev, A. McCrone, E. Musolino and L. Ranalder, *Renewables 2019 Global Status Report*, Report ISBN 978-3-9818911-7-1, 2019.
4. A. G. Fadeev, Y. A. Selinskaya, S. S. Kelley, M. M. Meagher, E. G. Litvinova, V. S. Khotimsky and V. V. Volkov, *J. Membr. Sci.*, 2001, **186**, 205-217.
5. J. Huang, *J. Membr. Sci.*, 2001, **192**, 231-242.
6. N. Qureshi and I. S. Maddox, *Food Bioprod. Process*, 2005, **83**, 43-52.
7. E. El-Zanati, E. Abdel-Hakim, O. El-Ardi and M. Fahmy, *J. Membr. Sci.*, 2006, **280**, 278-283.
8. V. García, E. Pongrácz, E. Muurinen and R. L. Keiski, *Desalination*, 2009, **241**, 201-211.
9. S.-Y. Li, R. Srivastava and R. S. Parnas, *J. Membr. Sci.*, 2010, **363**, 287-294.
10. S. Li, F. Qin, P. Qin, M. N. Karim and T. Tan, *Green Chemistry*, 2013, **15**, 2180.
11. S. Liu, G. Liu, X. Zhao and W. Jin, *J. Membr. Sci.*, 2013, **446**, 181-188.
12. H. Fan, N. Wang, S. Ji, H. Yan and G. Zhang, *J. Mater. Chem. A*, 2014, **2**, 20947-20957.
13. Z. Zhang, D. Chen, Y. Chen, Y. Hao, M. O. Tade and Z. Shao, *J. Membr. Sci.*, 2014, **472**, 10-18.
14. Y. Li, J. Shen, K. Guan, G. Liu, H. Zhou and W. Jin, *J. Membr. Sci.*, 2016, **510**, 338-347.
15. G. Merlet, F. Uribe, C. Aravena, M. Rodríguez, R. Cabezas, E. Quijada-Maldonado and J. Romero, *J. Membr. Sci.*, 2017, **537**, 337-343.
16. M. Matsumura, H. Kataoka, M. Sueki and K. Araki, *Bioprocess Engineering*, 1988, **3**, 93-100.
17. J. A. Gil, L. Túa, A. Rueda, B. Montaño, M. Rodríguez and D. Prats, *Desalination*, 2010, **250**, 997-1001.
18. A. P. Mariano, M. J. Keshtkar, D. I. P. Atala, F. Maugeri Filho, M. R. Wolf Maciel, R. Maciel Filho and P. Stuart, *Energy & Fuels*, 2011, **25**, 2347-2355.

19. C. Xue, X. Q. Zhao, C. G. Liu, L. J. Chen and F. W. Bai, *Biotechnol Adv*, 2013, **31**, 1575-1584.

20. V. Outram, C. A. Lalander, J. G. M. Lee, E. T. Davis and A. P. Harvey, *Bioresour. Technol.*, 2016, **220**, 590-600.

21. P. Jimenez-Bonilla and Y. Wang, *Crit. Rev. Biotechnol.*, 2018, **38**, 469-482.

22. J. W. Goodrum and M. A. Eiteman, *Bioresource Technology*, 1996, **56**, 55-60.

23. M. D. C. Claramonte, F. G. Vilchez and A. P. Vialard, *Thermochimica Acta*, 1993, **222**, 209-218.

24. J. H. Kim, S. H. Park, M. J. Lee, S. M. Lee, W. H. Lee, K. H. Lee, N. R. Kang, H. J. Jo, J. F. Kim, E. Drioli and Y. M. Lee, *Energy Environ. Sci.*, 2016, **9**, 878-884.

25. M. Cook, L. Peeva and A. Livingston, *Ind. Eng. Chem. Res.*, 2018, **57**, 730-739.

26. J. H. Kim, M. Cook, S. H. Park, S. J. Moon, J. F. Kim, A. G. Livingston and Y. M. Lee, *Green Chemistry*, 2018, **20**, 1887-1898.

27. J. H. Kim, S. J. Moon, S. H. Park, M. Cook, A. G. Livingston and Y. M. Lee, *J. Membr. Sci.*, 2018, **550**, 322-331.

28. H. B. Park, C. H. Jung, Y. M. Lee, A. J. Hill, S. J. Pas, S. T. Mudie, E. Van Wagner, B. D. Freeman and D. J. Cookson, *Science*, 2007, **318**, 254-258.

29. P. R. Brookes and A. G. Livingston, *J. Membr. Sci.*, 1995, **104**, 119-137.

30. S. D. Doig, A. T. Boam, A. G. Livingston and D. C. Stuckey, *J. Membr. Sci.*, 1999, **154**, 127-140.

31. R. Valadezblanco, F. Ferreira, R. Jorge and A. Livingston, *J. Membr. Sci.*, 2008, **317**, 50-64.

32. S. Sreekumar, Z. C. Baer, A. Pazhamalai, G. Gunbas, A. Grippo, H. W. Blanch, D. S. Clark and F. D. Toste, *Nat Protoc*, 2015, **10**, 528-537.

33. F. Muller, *U.S. Patent No. 3,933,647*, 1976.

34. M. Matsumura and H. Markl, *Biotechnology and bioengineering*, 1986, **28**, 534-541.

35. H. R. Acharya, S. A. Stern, Z. Z. Liu and I. Cabasso, *J. Membr. Sci.*, 1988, **37**, 205-232.

36. L. E. Black and R. C. Schucker, *U.S. Patent No. 4,962,271*, 1990.

37. F. J. Healy, J. R. Livingston, E. J. Mozeleski and J. G. Stevens, *U.S. Patent No. 5,298,669*, 1994.